analytical chemistry

pubs.acs.org/ac

Article

Hairpin-Spherical Nucleic Acids for Diagnosing COVID-19: a Simple Method to Generalize the Conventional PCR for Molecular Assays

Abbas Karami, Masoumeh Hasani,* Farid Azizi Jalilian, and Razieh Ezati

Cite This: *Anal. Chem.* 2021, 93, 9250−9257

Read Online

ACCESS | Metrics & More | Article Recommendations | Supporting Information

ABSTRACT: The COVID-19 pandemic revealed during the first global wave of this infectious disease that mass diagnostic testing was necessary to more rapidly detect infection in patients and control the pandemic. Therefore, extra research efforts to develop reliable and more accessible techniques for disease diagnosis are of supreme importance. Here, a target-responsive assembly of gold nanoparticle-core hairpin-spherical nucleic acids (AuNP-core H-SNAs) was implemented to modify the conventional polymerase chain reaction (PCR) assay for the "naked-eye" colorimetric detection of severe acute respiratory syndrome coronavirus 2 (SARS-CoV-2) RNA. Two hairpin DNA ligands are designed based on the two highly conserved regions within N and E genes of SARS-CoV-2 RNA by positioning two short palindromic arms (stem) on either side of a recognition sequence (loop). In the presence of a sequence-specific probe (activator), hairpin DNAs anchored to the surface of AuNPs unfold and expose the palindromic ends to the DNA-directed assembly of AuNPs. The sequence of the activator probes was chosen to be identical to the TaqMan probe in a real-time reverse transcription PCR (RT-PCR) assay for specifically targeting the N and E genes of SARS-CoV-2 RNA. They may either be degraded by the 5′-exonuclease activity of DNA polymerase during PCR cycles or stay intact depending on the presence or absence of the target template in the sample, respectively. Post-addition of H-SNA solutions to the final PCR products of some preconfirmed clinical samples for COVID-19 generated naked-eye-observable red and blue colors for positive and negative cases, respectively, with similar sensitivity to that of the real-time RT-PCR method.

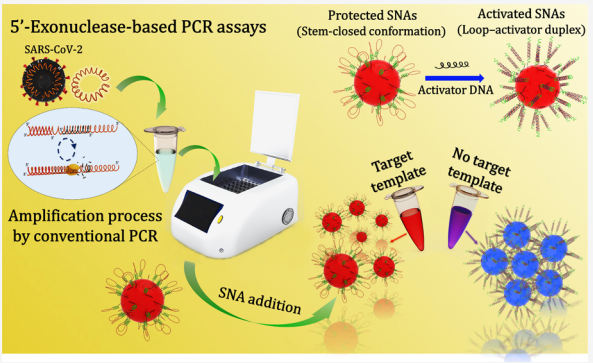

At the end of 2019, a major global health threat occurred by severe acute respiratory syndrome coronavirus 2 (SARS-CoV-2),[1] which caused the outbreak of COVID-19 disease, and a pandemic was announced by the World Health Organization (WHO). Early and accurate diagnostic testing of SARS-CoV-2 infection for large-scale population screening and subsequent management (i.e., isolation and tracking) of the infected cases could be one of the most urgent strategies to appropriate pandemic containment. Real-time reverse transcription polymerase chain reaction (real-time RT-PCR) is the most reliable method widely applied for the clinical diagnosis of COVID-19 infection.[2] In this method, the RNA viral genome is first transcribed into complementary DNA (cDNA) using the specific reverse transcriptase enzyme. The cDNA is then used as a template for the quantitative PCR reaction. The amplification process is performed using specific primer pairs and monitored by a fluorescence-labeled sequence-specific DNA probe (TaqMan probe). Probes for different target sequences of COVID-19, such as the spike protein, RNA-dependent RNA polymerase, and nucleocapsid protein have been designed soon after the SARS-CoV-2 genome was sequenced.[3−6]

The loop-mediated isothermal amplification (LAMP) method in which a molecular target is amplified at a constant temperature has also been widely employed for SARS-CoV-2 detection,[6−8] which provided a good alternative to PCR-based assays. Despite that, real-time RT-PCR is still the accepted gold standard for the diagnosis of COVID-19. However, in the COVID-19 pandemic crisis, the wide use of real-time PCR for large-scale population testing was limited due to the clinical shortage of SARS-CoV-2 molecular testing capacity and reagent kits in many countries. Thus, innovative, accessible, affordable, and reliable strategies for diagnosing COVID-19 are earnestly needed to reduce the demand for real-time PCR detection tests.[6,9−13]

Spherical nucleic acids (SNAs) are synthetic three-dimensional structures of nucleic acids made by the immobilization of a dense shell of DNA or RNA around a nanoparticle core.[14,15] SNAs exhibit unique properties different from those of both the individual nanoparticle core and nucleic acid shell.

Received: April 9, 2021
Accepted: June 8, 2021
Published: June 22, 2021

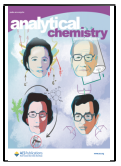

https://doi.org/10.1021/acs.analchem.1c01515
Anal. Chem. 2021, 93, 9250−9257

Colorimetric biosensor development based on AuNP-core SNAs is a theme that runs through merging the distance-dependent plasmonic properties of AuNPs and the programmable nature of DNA−DNA interactions.[16−19]

In the last 2 decades, the area of molecular diagnosis has attracted extensive interest in the use of nanomaterials in nucleic acid assays for many diseases. The role of AuNP-core SNAs as a biodetection system was first noticed in 1997[20] with the observation that SNAs can participate in a sequence-specific assembly process in the presence of target DNA. The simple target-directed aggregation of AuNP-core SNAs used these particles as DNA detection agents which acted by changing the color of the solution. DNA-programmable assembly of nanoparticles is an outstanding application of synthetic forms of DNA that can rationally be designed base-for-base through a four-letter alphabet of the nucleic acid language.

Mostly, DNA-based strategies for nanoparticle assembly are based on binary systems in which nanoparticles are separately functionalized with two different sequences of DNA.[21] However, in a single-component (unary) system, where each particle is able to bind to identical particles through self-complementarity of free palindromic tails, a simpler path to programed assembly can be provided. Palindromic sequences reveal a fascinating property called self-complementarity[13,22] because the complement of a palindrome is equal to itself. The existence of the self-complementary property at the free end of each nanoparticle−DNA conjugate induces nanoparticles to assemble into larger structures through head-to-head base pairing.

Most recently, we have developed two linker-based palindromic strategies for the colorimetric detection of human immunodeficiency virus-1 (HIV-1)[22] and SARS-CoV-2 nucleic acids.[13] In both strategies, a single-component assembly system based on bi-regional palindromic linkers, as both self-assembler and oligo-probe, has been designed. The detection of HIV-1 and SARS-CoV-2 was based on a six- and four-nucleotide (nt) palindromic sequence (with a GC content of 100%), respectively. In the strategy for diagnosing SARS-CoV-2, the amplification power of PCR and the programmability of the SNA assembly were combined through the 5′-exonuclease activity of the DNA polymerase to obtain a post-PCR colorimetric response. However, a drawback of linker-based single-component strategies in nucleic acid targeting is that finding proper sequences for designing a palindromic linker can be somewhat difficult, although palindromic repeats are found abundantly throughout a given genome.

In this study, the conventional PCR assay was modified for the "naked-eye" colorimetric detection of SARS-CoV-2 RNA by using AuNP-core hairpin-spherical nucleic acids (H-SNAs) to present another version of unary assembly formation of SNAs for diagnostic purposes. Positioning two short palindromic arms on either side of a recognition sequence (loop region) generates a stem-loop hairpin structure within DNA ligands attached onto AuNP-cores. DNA hairpins can serve as nanoparticle linkers after being activated in the presence of a sequence-specific probe (activator) complementary to the loop sequence. Two distinct hairpin SNA systems and the corresponding activator probes for the detection of SARS-CoV-2 were designed based on the TaqMan probes predominately used for targeting E and N genes of SARS-CoV-2 in the real-time RT-PCR method. Depending on whether the activator probes are digested or stayed undamaged by the 5′-exonuclease activity of DNA polymerase during the PCR amplification process, the postaddition of H-SNA solutions to the PCR products gives a proper eye-sensitive colorimetric response associated with the dispersed form (the red color) or the assembled form (the blue color) of the H-SNAs. This strategy can resolve the issue of finding an appropriate palindromic sequence within the nucleic acid targets for diagnostic purposes because the sequence of the palindromic arms is almost independent of the target genome and can be designed freely.

EXPERIMENTAL SECTION

Reagents and Chemicals. Detailed information on all the materials used in this work is available in the Supporting Information.

Hairpin-SNA Synthesis. AuNP cores were synthesized using the standard citrate reduction of $HAuCl_4$ in aqueous solution as described by Liu et al.[23] The prepared AuNP cores were then functionalized individually with two phosphorothioate (PS)-modified hairpin DNA designed for E and N genes based on the low-pH-assisted method developed by Liu and coworkers[24,25] with slight modifications. Experimental details on the synthesis and characterization of the synthesized H-SNAs are presented in the Supporting Information (Figure S1).

H-SNA Stability Analysis. The conjugate stability of the resulting hairpin-SNA particles was monitored after different days of storage (up to 45 days) both in a homogeneous aqueous solution at 4 °C and in the dried form. The DNA adsorption stability was evaluated by gel electrophoresis, fluorescence, and UV−vis techniques. The experimental details are available in the Supporting Information, and the results are shown in Figure S2.

UV−Vis Measurements and Transmission Electron Microscopy Analysis. The designed hairpin−SNA systems were characterized by UV−vis spectroscopy and transmission electron microscopy (TEM) images. All extinction spectra were collected in the range of 400−800 nm using a SPECORD 210 spectrophotometer (Analytik Jena) equipped with a Peltier temperature controller unit. TEM images were recorded on a Philips 208S transmission electron microscope at an electron energy of 100 kV. Details on the spectrophotometric measurements and TEM sample preparation are available in the Supporting Information.

Collection of Clinical Samples. This study was approved by the Bu Ali Sina University, Hamedan (Biomedical Research Ethics Committee). All clinical samples were received from a local clinical lab (Farzan Molecular and Pathobiology Laboratory, Hamedan, Iran). Written consent was obtained from all the suspected patients. The COVID-19 status of the samples was initially determined using a routine real-time RT-PCR kit for SARS-CoV-2 RNA detection (PCR-Fluorescence Probing, EUL 0493-141-00. Da An Gene Co.). The experimental details on the preparation of samples and RNA extraction are presented in the Supporting Information.

Post-PCR Colorimetric Test Algorithm. The presented assay platform in this work consists of a conventional RT-PCR step, followed by a colorimetric detection of PCR products based on H-SNA. The conventional RT-PCR step was performed on a Veriti Thermal Cycler from Thermo Fisher Scientific. Two specific primer pairs recommended by the WHO and the United States Centers for Disease Control and Prevention (CDC) for amplifying two different regions in the

https://doi.org/10.1021/acs.analchem.1c01515
Anal. Chem. 2021, 93, 9250−9257

Table 1. DNA Sequences Used in This Study

Description	Sequences and modifications (from 5′ to 3′)	Amplicon size	Ref.
E gene system		113	[27]
Hairpin DNA [a]	A*A*A*A*A*A*A*A*AAAGGCCCGAAGCGCAGTAAGGATGGCTAGTG AAGGCC		
Activator probe	ACACTAGCCATCCTTACTGCGCTTCG		
TaqMan probe [b]	FAM-ACACTAGCCATCCTTACTGCGCTTCG-BHQ1		
Forward primer	ACAGGTACGTTAATAGTTAATAGCGT		
Reverse primer	ATATTGCAGCAGTACGCACACA		
N gene system		72	[28]
Hairpin DNA [a]	A*A*A*A*A*A*A*A*AAAAGGCCGGTCCACCAAACGTAATGCGGGGT AAGGCC		
Activator probe	ACCCCGCATTACGTTTGGTGGACC		
TaqMan probe [b]	FAM- ACCCCGCATTACGTTTGGTGGACC -BHQ1		
Forward primer	GACCCCAAAATCAGCGAAAT		
Reverse primer	TCTGGTTACTGCCAGTTGAATCTG		

[a]Palindromic arms of the stem and flexor nucleotides are shown in green and blue, respectively; PS modification is denoted by "*". [b]FAM: 6-carboxyfluorescein; BHQ1: black hole quencher 1.

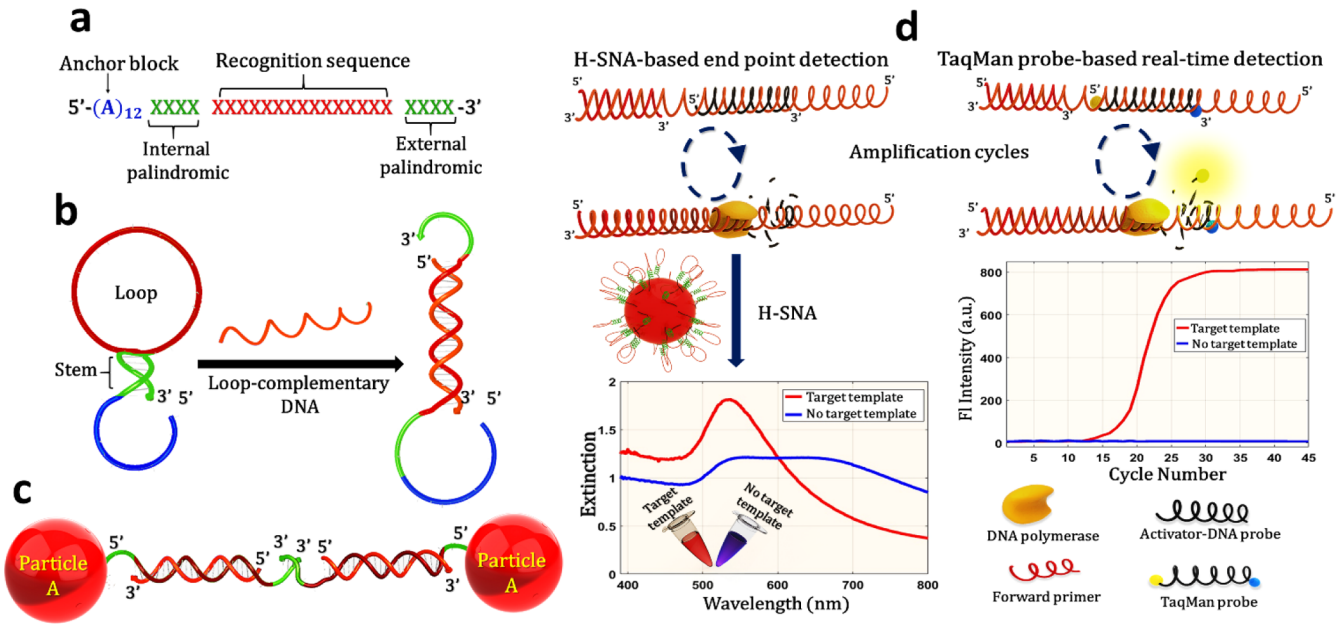

Figure 1. (a) Principal format of the hairpin DNA design for H-SNAs. (b) Conformational transition of hairpin DNAs from the stem-loop structure to the linear loop-activator duplex in the presence of the activator probe. (c) Single-component assembly of unfolded H-SNAs. (d) Schematic comparison of two 5′-exonuclease-based PCR assays. The color of the H-SNA solution remains red if DNA polymerase digests the activator probe after the whole PCR cycles, whereas the fluorescence signal is acquired owing to the digestion of the TaqMan probe during each cycle of the PCR reaction. The TaqMan probe is labeled with a fluorophore dye and a quencher dye as donor−acceptor pairs at the 5′ and 3′ ends, respectively.

E and N genes of SARS-CoV-2 (see Table 1) along with the designed specific probes (activators) were used. The reverse transcription and PCR amplification were performed in one step using a QIAGEN One-Step RT-PCR Kit (cat. number: 210210), according to the manufacturer's instructions. The amplification process was programed as follows: a 30 min/50 °C reverse transcription step, a 15 min/95 °C initial PCR activation step, then 45 cycles of 94 °C for 15 s, 55 °C for 45 s, and 72 °C for 60 s. The optimized volume and concentration of the components for the preparation of the master mixes are available in Table S1. Postcolorimetric testing was performed by adding 15 μL of PCR products to the H-SNA solution followed by addition of NaCl to the concentration of 380 mM (in total trial volume of 60 μL), and incubation at 60 °C for 1 min.

Real-Time RT-PCR Assay. The real-time RT-PCR reactions were also performed in the presence of the same primer pairs and probes used in the conventional RT-PCR for amplifying the amplicons of the E and N genes. Invitrogen SuperScript III Platinum One-Step RT-qPCR Kit (cat. number: 11732088) was used on a LightCycler 96 System from Roche Life Science with the following thermocycling conditions: 15 min at 48 °C for reverse transcription, 2 min at 94 °C for predenaturation followed by 45 cycles of 15 s at 94 °C, 30 s at 60 °C, and 1 min at 68 °C. The TaqMan probe in real-time RT-PCR, which is a dual-labeled oligonucleotide probe modified with both a fluorophore and a quencher, was identical in sequence to the activator probe in conventional RT-PCR, except that the activator probe was unlabeled.

https://doi.org/10.1021/acs.analchem.1c01515
Anal. Chem. 2021, 93, 9250−9257

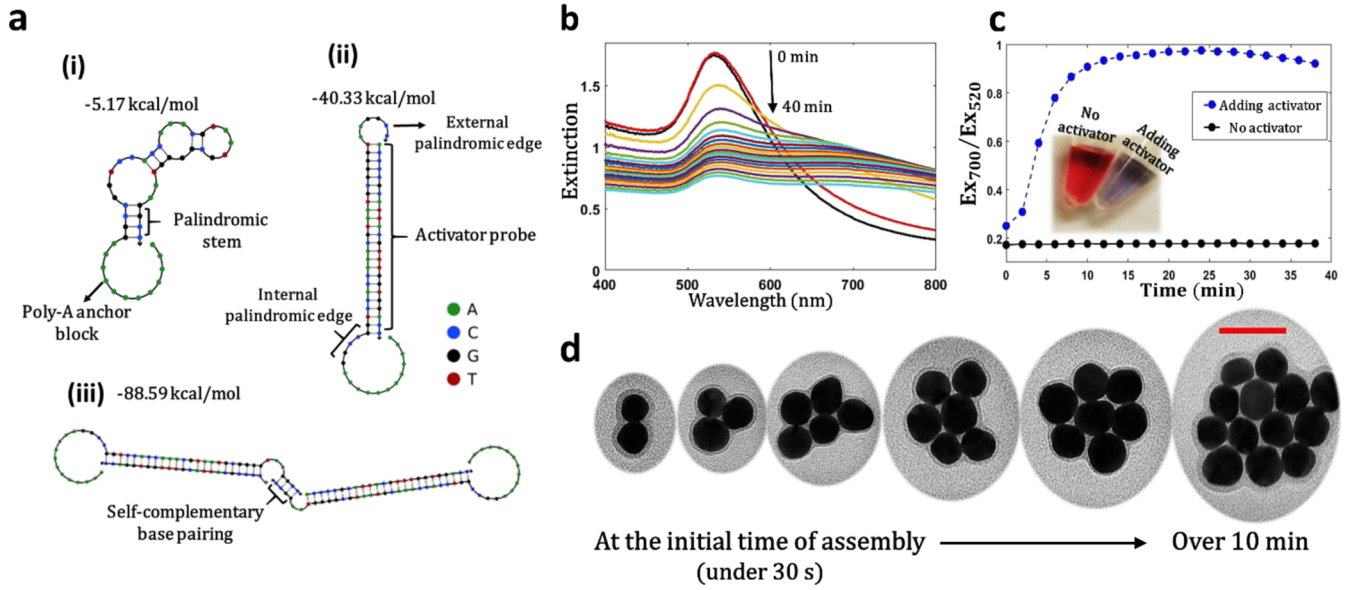

Figure 2. Characterization of the H-SNA system for the N gene. (a) Polymer graphs simulated by NUPACK analysis algorithms representing the expected secondary structures of the hairpin DNA. (i) Closed state corresponding to a stem-loop hairpin structure, (ii) open state corresponding to the loop-activator duplex, and (iii) secondary structure corresponding to the sticky-end base pairing that guided a single-component assembly. The MFEs are shown on the top of each secondary structure. (b) UV−vis spectral monitoring of a single-component assembly formation over time with a fixed time interval of 2 min (in a total volume of 60 μL of 10 mM HEPES buffer, pH = 7.6, containing 8 nM SNAs, 25 nM activator probe, and 380 mM NaCl). (c) Changes in the Ex_{700}/Ex_{520} ratio as a function of time. The photographs representing the color of the SNA solution in the presence and in the absence of the activator probe are shown as the inset (the pictures were taken using a digital camera, Nikon D7200, 10 min after the pre-incubation step at 60 °C). (d) TEM images as a visual stopwatch for the characterization of the assembly growth evolution (from the primary seed formation step to the extension step of the flower-like configuration; scale bar, 25 nm).

RESULTS AND DISCUSSION

Palindromic-Based H-SNAs for the Colorimetric Detection of PCR Products. Palindromic-based hairpin DNAs are able to form a stem-loop hairpin structure when the two self-complementary palindromic arms fold and self-hybridize. The hairpin DNAs designed for the current study consisted of four functional regions: anchor block, internal palindromic sequence, a target specific sequence (recognition sequence), and external palindromic sequence (Figure 1a). Immobilization of a dense layer of the palindromic-based hairpin DNA onto AuNPs via its anchor block results in a class of AuNP-core SNAs which we termed H-SNAs. Once AuNPs were functionalized with palindromic-based hairpin DNAs, SNAs can be programed to either stay in a stably dispersed state or form predefined assemblies through folding and unfolding the hairpin structure, respectively. The identical internal and external self-complementary palindromic sequences on either side of the recognition sequence simply generate a stem-loop hairpin structure in its free form by intramolecular hybridization (Figure 1b). However, hybridization of an oligonucleotide complementary to the loop sequence, called the activator DNA, disrupts the stem-loop structure. This causes the external palindromic arms in the adjacent SNAs to become available to act as the sticky ends for interparticle binding and induce single-component assembly (Figure 1c). This assembly formation is expected to make an intense red-to-blue color change. Activator probes in the current study face the same enzymatic activity of DNA polymerase during cycles of conventional PCR as a TaqMan probe in real-time PCR. Activators are complementary to the sequence within the template and hybridized with the target sequence downstream of one of the primers, that is, the region that will be amplified. If the activator DNA is specifically selected to bind a sequence within a specific amplicon of the target template, it will be degraded by the 5′-exonuclease activity of the DNA polymerase during PCR cycles when the enzyme encounters a double-stranded region. Then, by adding the H-SNA solution to the final PCR product, as a post-PCR amplicon detection step, the colloidal form and the red color of the H-SNA solution in the suspension will be maintained. Because the digested activator DNA in the course of the amplification process is no longer able to open the hairpin structure of the attached DNA layer on AuNPs. In other words, the stable red color of the H-SNA solution, after being added into the PCR products, indicates the presence of the correct DNA template in the PCR reaction. However, the self-assembly of H-SNAs in post-PCR colorimetric detection is expected if the target template is absent in the sample and the activator probe leaves intact during the PCR amplification. A graphical comparison between the post-PCR colorimetric detection and the TaqMan-based real-time monitoring of amplification products is shown in Figure 1d.

The SARS-CoV-2 Genome as a Template for Designing H-SNAs. SARS-CoV-2 is a positive-sense, single-stranded, enveloped RNA coronavirus with one of the largest known RNA viral genomes (~29.8 kb in size).[26] Generally, the highly conserved areas in viral genomes are targeted in designing the specific primers and probes for real-time PCR assays. Three regions of SARS-CoV-2 have been considered as reliable RT-PCR targets including the RNA-dependent RNA polymerase (RdRp) gene, nucleocapsid protein (N) gene, and envelope protein (E) gene. Following the recommendations from the WHO[27] and the CDC,[28] we implemented our strategy by designing two distinct H-SNA systems for directly targeting E and N genes as used in real-time RT-PCR assays for detecting SARS-CoV-2. As the designed H-SNAs are supposed to detect

https://doi.org/10.1021/acs.analchem.1c01515
Anal. Chem. 2021, 93, 9250−9257

PCR products, the activator oligonucleotide sequence should be chosen to be complementary to any region within the amplicon except for the position of the primer binding sites just like the TaqMan probe in real-time RT-PCR. Hence, the sequences of TaqMan probes that have formerly been designed for targeting E and N genes in real-time RT-PCR were selected as the activator probe sequence along with the relevant specific primers (Table 1).

By having these two activator probes, we needed to make H-SNAs by functionalizing gold nanoparticles with DNA sequences capable of forming a hairpin structure. The loop of the DNA hairpin must be complementary to the activator probe sequence and the stem of the DNA hairpin designed with two identical 4-nt palindromic sequences (5′-GGCC-3′), which were added on either side of the loop sequence. In order to enhance the flexibility of the designed single-component system during self-assembly, the external palindromic tail and the loop sequence were separated by two nonbinding adenosines (A). To enable attaching hairpin DNA to AuNPs, a 12-nt poly-A was added at its 5′ end as an anchor block such that its first eight phosphates were tandemly replaced by PS. The PS is an internucleotidic modification in which a sulfur atom is substituted for one of the nonbridging oxygen in the linkage phosphates.[29] All sequences of primers, probes, and both designed hairpin DNAs are listed in Table 1.

Secondary Structure Analysis of Designed Hairpin DNAs. Here, NUPACK Analysis Algorithms were used for the prediction of secondary structures induced by intramolecular base pairing of the hairpin DNA alone and intermolecular hybridization between the loop region of hairpin DNA and the activator probe. NUPACK analysis algorithms are able to provide the polymer graphs for the possible secondary structure of one or more interacting nucleic acid strands with minimum free energy (MFE).[30,31] The polymer graph representation of the secondary structures attributed to the closed hairpin state, the loop-activator duplex open state, and the assembly-guided structure is depicted in Figure 2a and S3a for N gene and E gene, respectively. NUPACK results demonstrated that both the designed hairpin DNAs for N and E genes could successfully form the expected secondary structures in the absence and presence of the relevant activator probes, eventually leading to the self-complementary assembly.

Spectroscopy- and Electron Microscopy-Based Characterization. Kinetics of the activated single-component assembly formation of the both designed H-SNAs for N and E genes was primarily monitored by UV−vis spectroscopy in the presence of the relevant activator probes (Figures 2b and S3b for N and E genes, respectively). The most important spectrophotometric index for monitoring self-assembly processes of AuNP-core SNAs is a simultaneous decrease in the extinction around 520 nm and an increase in the extinction at around 650−750 nm. As shown in Figures 2c (and S3c), the rate of change of the Ex_{700}/Ex_{520} ratio is relatively fast in the presence of the activator probe; whereas, in the absence of the activator probe, there is no significant change in the Ex_{700}/Ex_{520} ratio. Moreover, the self-assembly processes of both H-SNAs were accompanied by a fast-distinct color change that could provide an eye-sensitive colorimetric response (inset of Figures 2c and S3c for N and E genes, respectively).

Next, the assembly growth of the H-SNA systems was evaluated over time using a TEM technique (Figure 2d). The ability to form a flower-like configuration may be considered as an interesting feature of single-component assembly systems. Once the hairpin stem is opened, upon activator recognition, the external palindromic end is pushed to the edge of the particles and acts as a free sticky end allowing different SNAs to bind to one another with equal possibility. The flower-like configuration suggests that each unfolded H-SNA tends to symmetrically complete its surrounding capacity by connecting to the identical SNA particles.

Assay Performance Optimization. To achieve the best colorimetric response associated with the hairpin structure-based single-component assembly of AuNPs, the H-SNA performance must be optimized in two aspects. The highest ionic strength that sustains the colloidal SNAs stable and the lowest concentration of the activator probe that leads to sufficient color change must be determined. All optimization processes were performed via monitoring kinetic spectral data (the details of experimental conditions are available in the Supporting Information). First, the colloidal stability of the H-SNA solution was investigated at various concentrations of NaCl at a constant concentration of 0.625 mM $MgCl_2$ (due to adding 15 μL of the PCR product containing 2.5 mM $MgCl_2$ to H-SNA solutions in postcolorimetric detection step results in a final concentration of 0.625 mM $MgCl_2$ in a total volume of 60 μL). As shown in Figure S4a, at greater than 400 mM NaCl, the Ex_{700}/Ex_{520} ratio of the SNA solution started to increase, which was a consequence of the loss of colloidal stability due to the aggregation of SNAs at high ionic strength. Therefore, 380 mM was chosen as the optimum concentration of NaCl to ensure the stability of SNAs. To optimize the amount of the activator probe, the kinetics of self-assembly formation was monitored with various amounts of the activator probe in the range of 25−12 nM at a NaCl concentration of 380 mM after 1 min of annealing at a temperature of over 60 °C. Overall, the best colorimetric response was obtained with 22 nM of the activator probe (for both N and E genes, Figure S4b).

To determine the optimal PCR annealing temperature, different temperatures (55 to 60 °C) were tested for the cycling program, and the PCR products were then analyzed by gel electrophoresis. The results showed two single bands of the expected size for both amplicons of N and E genes at a temperature of 55 °C (Figure S4c).

Colorimetry-Based RT-PCR assay for COVID-19. Two singleplex amplification formats for targeting E and N genes were separately performed using the corresponding specific primer pairs and activator probes. The E gene system is tried as the first-line screening test.[2,6] If the color of the added H-SNA in the post-PCR colorimetric test remains red, which is presumably an indication of a positive result, the N system is also performed as the confirmatory test to ensure that the initial test is a true positive. A gel electrophoretic analysis on singleplex PCR products of both N- and E-gene amplicons corresponding to two confirmed positive (with a low Ct value) and negative samples represents single bands of the expected size for the positive sample and no band for the negative control one (Figure 3a). Next, 15 μL of singleplex PCR products was added individually to H-SNA solutions for E and N genes in a total volume of 60 μL, followed by annealing at 60 °C for 1 min. As shown in Figure 3b, the color of the positive samples remains red, whereas negative control samples show a distinct red-to-purple color change for both E and N gene trial solutions in a few minutes.

Performance Criteria for the Assay. To ensure that the proposed method is reliable and accurate, we analyzed 72

https://doi.org/10.1021/acs.analchem.1c01515
Anal. Chem. 2021, 93, 9250−9257

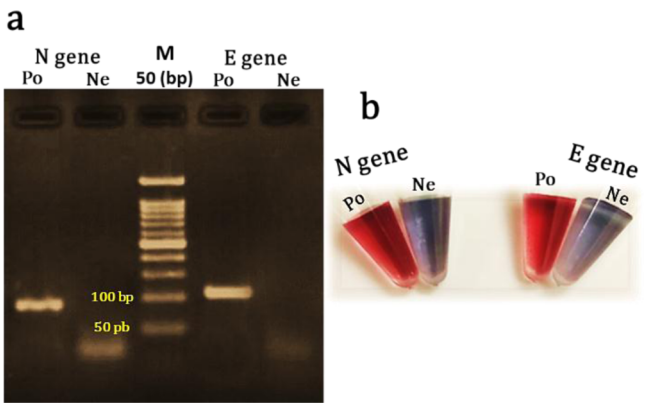

Figure 3. (a) Gel electrophoretic analysis of conventional PCR products obtained from the specific primer–probe sets associated with the E- and N-gene amplicons after 45 cycles of amplification. (b) Photograph representing post-PCR colorimetric detection of the samples in the gel electrophoresis experiment. DNA marker: M, positive: Po, and negative: Ne.

clinically confirmed samples (including 30 positives, 18 low-positives with a cycle threshold (Ct) value between 34 to 38 and 24 negatives) by our proposed assay (i.e., conventional PCR coupled with a H-SNA colorimetric assay). The conventional RT-PCR is performed on the extracted RNA samples, as described in the Experimental Section. The obtained PCR products were then tested after being added to the H-SNA solutions and annealing at 60 °C. As shown in Table 2 and Figure 4, 100% of the positive, 94% of the low-positive (17 out of 18), and 96% of the negative samples (23 out of 24) returned the correct results.

Table 2. Validation of the Assay Accuracy (Positive: Po and Negative: Ne)

calibrator	no.	E gene		N gene	
		Po	Ne	Po	Ne
positive[a]	30	30		30	
low positive[b]	18	17		17	
negative	24		23		23

[a]Confirmed cases by the real-time RT-PCR method with a Ct value lower than 35. [b]Confirmed cases by the real-time RT-PCR method with a weak Ct value (between 35 and 39).

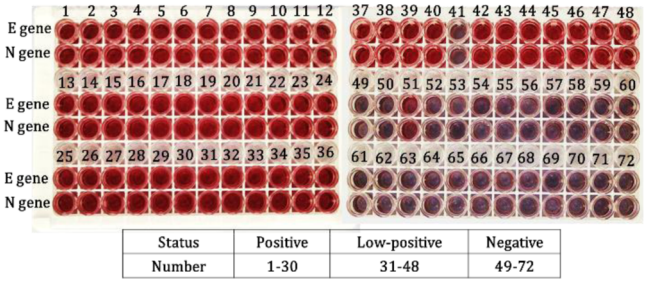

Figure 4. Photograph representing the results of the post-PCR colorimetric assay on 72 clinical samples for confirming the accuracy of the assay.

To evaluate the limit of detection of the assay, a synthetic ssDNA strand (72-nt) with an identical sequence to the amplicon of the N gene was used. The sequences of E and N gene amplicons, along with their primer and probe binding sites are shown in Table S2. Conventional PCR amplification (without reverse transcription step) was performed on a series of diluted synthetic ssDNA (6000 to 3 copy numbers per reaction) by using the primer–probe set of the N gene. Each sample was tested in triplicate. As shown in Figure S5, the lowest concentration of the synthetic ssDNA amplicon that yielded three stable positive signals from the triplicate assay is six copies of ssDNA per reaction.

To investigate the specificity of H-SNA activation, four synthetic mismatched activators were used by imposing one (or more) nucleotide mismatch(es) into the probe sequence. The change of the Ex_{700}/Ex_{520} ratio of solution of H-SNA designed for the N gene as a function of time in the presence of the mismatched activators (under the experimental condition presented in Figure 2b) revealed no activated assembly for four- and three-nucleotide mismatched probes (Figure S6). Although one- and two-nucleotide mismatches showed slight assembly formation in the spectrophotometric measurement, their kinetics was significantly different from that of a full matched activator and no naked-eye visible colorimetric change was observed. Therefore, it is notable to say that the specific activation of H-SNAs prevents false negative diagnosis.

The reproducibility of the assay was evaluated in two ways. First, three confirmed low-positive and three confirmed negative samples were individually amplified for both N and E gene systems in triplicate. The three PCR products obtained from each amplicon were then tested by freshly prepared H-SNAs for N and E gene systems. All 18 low-positive trials (nine for E and N genes each) yielded a positive signal and all 18 negative trials (nine for E and N genes each) showed no positive signal. Second, the reproducibility of the assay was assessed by the consistency of the post-PCR colorimetric results related to the reproducible H-SNA synthesis. For doing this, the H-SNAs designed for both N and E genes were prepared many times repeatedly under the same condition on the same and different days. They were added to the relevant PCR products corresponding to a low positive sample. There was no difference in the colorimetric responses corresponding to both methods of experimental replication.

To determine the concordance level of the sensitivity of the presented assay and the real-time RT-PCR method, the obtained results of testing a 10-fold serial dilution of three positive samples (range of dilution factor: 10^0 to 10^5) were compared in the two methods. In Table 3, the results obtained from the post-PCR colorimetric and the real-time RT-PCR methods are expressed in the form of Boolean answers (+ or −) and Ct values, respectively. For further comparison, a photograph of the post-PCR colorimetric detection for the five steps of the serial dilutions of all three samples and the real-time RT-PCR amplification curves for the sample no. 3 is shown in Figure S7. Collectively, the H-SNA-based post-PCR colorimetric method, compared with the real-time RT-PCR method, demonstrated the same detection sensitivity for sample no. 1 and 2 and 10-fold better detection sensitivity for sample no. 3.

Technical Comparison of LAMP, Real-Time RT-PCR, and H-SNA-Based PCR Methods. In comparison to the real-time RT-PCR technique which requires sophisticated equipment with well-trained personnel, LAMP has been reported to have many advantages such as amplification at a constant temperature, elimination of a thermal cycler, and a shorter assay time along with high sensitivity and specificity. This

https://doi.org/10.1021/acs.analchem.1c01515
Anal. Chem. 2021, 93, 9250–9257

Table 3. Sensitivity Comparison of the Post-PCR Colorimetric and Real-Time RT-PCR Methods

dilution factor	results											
	real-time RT-PCR (Ct value)[a]						post-PCR colorimetric method[b]					
	no. 1		no. 2		no. 3		no. 1		no. 2		no. 3	
	E	N	E	N	E	N	E	N	E	N	E	N
1	22.86	22.67	24.74	24.58	25.76	25.58	+	+	+	+	+	+
10	25.38	25.18	27.6	27.34	29.32	29.18	+	+	+	+	+	+
100	28.37	28.14	30.66	30.41	32.87	32.69	+	+	+	+	+	+
1000	31.44	31.26	33.74	33.52	36.28	36.14	+	+	+	+	+	+
10,000	34.71	34.58	36.82	36.63	NA	NA	+	+	+	+	+	+
100,000	38.34	38.19	NA	NA	NA	NA	+	+	−	−	−	−

[a]Ct value of more than 40 is reported as "NA" (not applicable) because it is not clinically applicable to such a low level of viral load. [b]Positive and negative results are indicated by "+" and "−", respectively.

method when coupled with reverse transcription can also amplify RNA sequences with high efficiency. These advantages make LAMP more suitable for point-of-care applications.[32] However, the complicated design of multiple primers and the inability to multiplex assays in a single sample are considered as some challenges in this method.[33]

In the proposed method (i.e., H-SNA-based PCR), the main device is a simple thermal cycler which can be considered as accessible and affordable laboratory equipment. Therefore, the method is technically simple. The visual detection method is a simple color change which is similar to the LAMP. In combination with the capability of adapting TaqMan probes for designing the hairpin SNAs and instantaneous attachment of PS-DNA onto AuNPs, anyone with basic skills of clinical manipulation can be able to operate all the steps successfully. Moreover, our outlook ahead is multiplex diagnosis of viral infectious diseases with the proposed system which is more developed for PCR than for LAMP. Some technical differences between the LAMP, real-time RT-PCR, and H-SNA-based PCR techniques are summarized in Table S3.

CONCLUSIONS

The proposed strategy is a further illustration of the capability of palindromic sequences to be exploited in diagnostic analysis. We used the switchable feature of the palindromic-based stem-loop structure for inducing a target-responsive single-component assembly of SNAs which provides a simple colorimetric response. Through the 5′-exonuclease activity of the DNA polymerase, hairpin-SNA probes can be simply coupled with conventional PCR, which requires minimal laboratory equipment (a simple thermal cycler). Good sensitivity and specificity in conjunction with simple operation can make H-SNAs a reliable biosensing method for the detection of viral nucleic acids. Due to public health interest in diagnosing infectious diseases using simple, accessible, and affordable laboratory equipment, the biosensing method based on H-SNA may be envisioned to have widespread applications in the diagnosis of COVID-19 and other infectious diseases.

ASSOCIATED CONTENT

Supporting Information

The Supporting Information is available free of charge at https://pubs.acs.org/doi/10.1021/acs.analchem.1c01515.

Experimental details on the synthesis, characterization, and stability analysis of AuNP-core H-SNAs; UV−vis kinetic measurements and TEM analysis; results on assay performance optimization, assay detection limit, and evaluation of the specificity of H-SNA activation; comparison of the sensitivity of the presented assay and the real-time RT-PCR, optimized concentrations and volumes of reaction components for conventional RT-PCR, the sequences of E and N gene amplicons, and information on the technical comparison of the proposed method with LAMP and RT-qPCR methods (PDF)

AUTHOR INFORMATION

Corresponding Author

Masoumeh Hasani − *Faculty of Chemistry, Bu-Ali Sina University, Hamedan 65174, Iran;* orcid.org/0000-0002-2223-0806; Email: hasani@basu.ac.ir

Authors

Abbas Karami − *Faculty of Chemistry, Bu-Ali Sina University, Hamedan 65174, Iran*

Farid Azizi Jalilian − *Department of Medical Virology, Faculty of Medicine, Hamedan University of Medical Sciences, Hamedan 6517619654, Iran*

Razieh Ezati − *Department of Molecular Diagnosis, Farzan Molecular and Pathobiology Laboratory, Hamedan 6515638377, Iran*

Complete contact information is available at: https://pubs.acs.org/10.1021/acs.analchem.1c01515

Author Contributions

A.K. designed and performed the experiments, drafted the manuscript, and designed the figures. M.H. supervised the project and wrote the current version of the manuscript. F.A.J. designed and directed the molecular experiments that were conducted. R.E. performed molecular experiments such as RNA extraction and PCR reactions.

Notes

The authors declare no competing financial interest.

ACKNOWLEDGMENTS

The authors are grateful to Bu-Ali Sina University Research Council for financial support.

REFERENCES

(1) Zhu, N.; Zhang, D.; Wang, W.; Li, X.; Yang, B.; Song, J.; Zhao, X.; Huang, B.; Shi, W.; Lu, R. *N. Engl. J. Med.* **2020**, *382*, 727−733.
(2) Corman, V. M.; Landt, O.; Kaiser, M.; Molenkamp, R.; Meijer, A.; Chu, D. K. W.; Bleicker, T.; Brünink, S.; Schneider, J.; Schmidt, M. L. *Eurosurveillance* **2020**, *25*, 2000045.

(3) Chu, D. K. W.; Pan, Y.; Cheng, S. M. S.; Hui, K. P. Y.; Krishnan, P.; Liu, Y.; Ng, D. Y. M.; Wan, C. K. C.; Yang, P.; Wang, Q.; Peiris, M.; Poon, L. L. M. *Clin. Chem.* **2020**, *66*, 549−555.
(4) Chan, J. F.-W.; Yip, C. C.-Y.; To, K. K.-W.; Tang, T. H.-C.; Wong, S. C.-Y.; Leung, K.-H.; Fung, A. Y.-F.; Ng, A. C.-K.; Zou, Z.; Tsoi, H.-W.; Choi, G. K.-Y.; Tam, A. R.; Cheng, V. C.-C.; Chan, K.-H.; Tsang, O. T.-Y.; Yuen, K.-Y. *J. Clin. Microbiol.* **2020**, *58*, e00310−e00320.
(5) Feng, W.; Newbigging, A. M.; Le, C.; Pang, B.; Peng, H.; Cao, Y.; Wu, J.; Abbas, G.; Song, J.; Wang, D.-B.; Cui, M.; Tao, J.; Tyrrell, D. L.; Zhang, X.-E.; Zhang, H.; Le, X. C. *Anal. Chem.* **2020**, *92*, 10196−10209.
(6) Udugama, B.; Kadhiresan, P.; Kozlowski, H. N.; Malekjahani, A.; Osborne, M.; Li, V. Y. C.; Chen, H.; Mubareka, S.; Gubbay, J. B.; Chan, W. C. W. *ACS Nano* **2020**, *14*, 3822−3835.
(7) Cui, F.; Zhou, H. S. *Biosens. Bioelectron.* **2020**, *165*, 112349.
(8) Thompson, D.; Lei, Y. *Sens. Actuators Rep.* **2020**, *2*, 100017.
(9) Moitra, P.; Alafeef, M.; Dighe, K.; Frieman, M. B.; Pan, D. *ACS Nano* **2020**, *14*, 7617−7627.
(10) Norman, M.; Gilboa, T.; Ogata, A. F.; Maley, A. M.; Cohen, L.; Busch, E. L.; Lazarovits, R.; Mao, C.-P.; Cai, Y.; Zhang, J.; Feldman, J. E.; Hauser, B. M.; Caradonna, T. M.; Chen, B.; Schmidt, A. G.; Alter, G.; Charles, R. C.; Ryan, E. T.; Walt, D. R. *Nat. Biomed. Eng.* **2020**, *4*, 1180−1187.
(11) Qiu, G.; Gai, Z.; Tao, Y.; Schmitt, J.; Kullak-Ublick, G. A.; Wang, J. *ACS Nano* **2020**, *14*, 5268−5277.
(12) Talebian, S.; Wallace, G. G.; Schroeder, A.; Stellacci, F.; Conde, J. *Nat. Nanotechnol.* **2020**, *15*, 618−621.
(13) Karami, A.; Hasani, M.; Azizi Jalilian, F.; Ezati, R. *Sens. Actuators, B* **2021**, *328*, 128971.
(14) Fong, L.-K.; Wang, Z.; Schatz, G. C.; Luijten, E.; Mirkin, C. A. *J. Am. Chem. Soc.* **2018**, *140*, 6226−6230.
(15) Cutler, J. I.; Auyeung, E.; Mirkin, C. A. *J. Am. Chem. Soc.* **2012**, *134*, 1376−1391.
(16) Li, D.; Song, S.; Fan, C. *Acc. Chem. Res.* **2010**, *43*, 631−641.
(17) Liu, J.; Cao, Z.; Lu, Y. *Chem. Rev.* **2009**, *109*, 1948−1998.
(18) Zhao, W.; Brook, M. A.; Li, Y. *ChemBioChem* **2008**, *9*, 2363−2371.
(19) Rosi, N. L.; Mirkin, C. A. *Chem. Rev.* **2005**, *105*, 1547−1562.
(20) Elghanian, R.; Storhoff, J. J.; Mucic, R. C.; Letsinger, R. L.; Mirkin, C. A. *Science* **1997**, *277*, 1078−1081.
(21) Laramy, C. R.; O'Brien, M. N.; Mirkin, C. A. *Nat. Rev. Mater.* **2019**, *4*, 201−224.
(22) Karami, A.; Hasani, M. *Anal. Chim. Acta* **2020**, *1102*, 119−129.
(23) Liu, J.; Lu, Y. *Nat. Protoc.* **2006**, *1*, 246−252.
(24) Zhou, W.; Wang, F.; Ding, J.; Liu, J. *ACS Appl. Mater. Interfaces* **2014**, *6*, 14795−14800.
(25) Zhang, X.; Servos, M. R.; Liu, J. *J. Am. Chem. Soc.* **2012**, *134*, 7266−7269.
(26) Wu, A.; Peng, Y.; Huang, B.; Ding, X.; Wang, X.; Niu, P.; Meng, J.; Zhu, Z.; Zhang, Z.; Wang, J.; Sheng, J.; Quan, L.; Xia, Z.; Tan, W.; Cheng, G.; Jiang, T. *Cell Host Microbe* **2020**, *27*, 325−328.
(27) Corman, V.; Bleicker, T.; Brünink, S.; Drosten, C.; Zambon, M. *Diagnostic Detection of 2019-nCoV by Real-Time RT-PCR*; World Health Organization, January 2020; p. 17.
(28) Lu, X.; Wang, L.; Sakthivel, S. K.; Whitaker, B.; Murray, J.; Kamili, S.; Lynch, B.; Malapati, L.; Burke, S. A.; Harcourt, J. *Emerging Infect. Dis.* **2020**, *26*, 1654−1665.
(29) Verma, S.; Eckstein, F. *Annu. Rev. Biochem.* **1998**, *67*, 99−134.
(30) Dirks, R. M.; Pierce, N. A. *J. Comput. Chem.* **2003**, *24*, 1664−1677.
(31) Dirks, R. M.; Pierce, N. A. *J. Comput. Chem.* **2004**, *25*, 1295−1304.
(32) Scott, A. T.; Layne, T. R.; O'Connell, K. C.; Tanner, N. A.; Landers, J. P. *Anal. Chem.* **2020**, *92*, 13343−13353.
(33) Martzy, R.; Kolm, C.; Krska, R.; Mach, R. L.; Farnleitner, A. H.; Reischer, G. H. *Anal. Bioanal. Chem.* **2019**, *411*, 1695−1702.

https://doi.org/10.1021/acs.analchem.1c01515
Anal. Chem. 2021, 93, 9250−9257